Techniques for Visualization of Cavern Boundaries in Opaque Industrial Mixing Systems

M. J. H. Simmons and I. Edwards
Johnson Matthey Technology Centre, PO Box 1, Belasis Avenue, Billingham, Cleveland TS23 1LB, United Kingdom
School of Chemical Engineering, University of Birmingham, Edgbaston, Birmingham B15 2TT, United Kingdom

J. F. Hall
Johnson Matthey Technology Centre, PO Box 1, Belasis Avenue, Billingham, Cleveland TS23 1LB, United Kingdom

X. Fan and D. J. Parker
School of Physics and Astronomy, University of Birmingham, Edgbaston, Birmingham B15 2TT, United Kingdom

E. H. Stitt
Johnson Matthey Technology Centre, PO Box 1, Belasis Avenue, Billingham, Cleveland TS23 1LB, United Kingdom

DOI 10.1002/aic.11889
Published online July 23, 2009 in Wiley InterScience (www.interscience.wiley.com).

In the agitation of complex fluids, the avoidance of caverns is essential for successful blending. Electrical resistance tomography (ERT) and positron emission projection imaging, which can both image within opaque fluids, have been assessed for visualization of cavern boundaries. A vessel of diameter, T = 154 mm, equipped with a single 57 mm diameter six bladed 45° down pumping pitched blade disc turbine formed the test system. The fluid used was aqueous solution of carbopol 940. Both techniques were used to detect and image caverns at Re from 20–86.6 and compared with optical images. Reasonable agreement on the maximum cavern heights and widths were obtained, with the taller and narrower caverns obtained via 3D ERT measurements being attributed to artifacts of the method and interactions between the polymer and tracer. Caverns were also detectable using a robust linear ERT array, which has potential for use within industrial systems. © 2009 American Institute of Chemical Engineers *AIChE J,* 55: 2765–2772, 2009

Keywords: electrical resistance tomography, positron emission tomography, caverns, stirred tanks, non-Newtonian fluids

Introduction

During the agitation of viscoplastic fluids in a stirred vessel, it is possible to generate an agitated volume around the impeller, defined as a cavern, surrounded by a stagnant region where the shear stress is insufficient to overcome the apparent yield stress of the fluid. A similar phenomenon may be observed in highly shear-thinning, or pseudoplastic systems, leading to the creation of "pseudo-caverns." Clearly, the avoidance of these caverns is essential to ensure vessel homogeneity and successful mixing. The majority of published work has focused on visualization using model

Correspondence concerning this article should be addressed to M. J. H. Simmons at m.j.simmons@bham.ac.uk

transparent fluid, where the size of the cavern has been shown to be dependent on fluid properties, impeller characteristics, and the rotational speed and torque of the impeller.[1]

Although this work has been useful to develop fundamental understanding, it does not address the problem of analyzing industrial systems containing opaque multiphase fluids, which often possess complex rheology. Only a few experimental studies exist for the determination of the extent of caverns within stirred vessels containing opaque fluids. Earlier work used invasive methods to measure the cavern size by moving the impeller to the liquid surface or vessel wall and observing the flow. An alternative semi-invasive technique employs the injection of glitter into the cavern and the fluid is then frozen,[1] enabling cavern dimensions to be obtained by dissection. However, this technique has only been applied to caverns formed in an unbaffled tank, presumably to allow easier access to the frozen solid for postprocessing.

Some published studies use specialist laboratory equipment to perform noninvasive measurements in-situ, although their application to date is limited. Medical X-ray apparatus, with a maximum field of view of 230 mm, has been used to study mixing patterns in solutions of xanthan gum by addition of a barium tracer into the cavern.[2] An Ultrasonic Doppler Velocimetry (UDV) probe has been used to obtain velocities in pulp suspension mixing[3]; however, a number of measurements for different probe positions are required to reconstruct a three-dimensional flow field, as only the component of the particle velocity along the axis of transmission of the ultrasound can be measured.

This study evaluates the applicability of two imaging techniques which are suitable for opaque materials in industrial systems, Electrical Resistance Tomography (ERT), and Positron Emission Projection Imaging (PEPI). To enable direct comparison with conventional visualization techniques, the results were obtained using a transparent aqueous polymer solution. ERT has been applied previously to image macromixing within large stirred vessels containing low viscosity fluids[4] and in pharma applications to obtain flow behavior and solids distribution in multiphase complex systems.[5] Lab-scale ERT experiments on caverns using xanthan gum have been performed recently and compared with CFD simulations.[6] In recent work, PEPI has been applied by geologists to determine dispersion in porous rock samples.[7]

Materials and Methods

The vessels used in the experiments had a diameter, T of 154 mm and were equipped with a single six bladed 45° down pumping pitched blade disc turbine (6-PBDT-d) of diameter, $D = 57$ mm. The impeller clearance, C, was $0.4T$ and the vessels were filled with 3.5 l of fluid giving a height, $H = 1.2T$. The experiments were performed at rotational speeds, N of 58, 80, 162, 207, and 310 rpm corresponding to the same Reynolds numbers as a previous study on the development of caverns using a down-pumping pitched blade turbine.[8]

The fluid used was an aqueous solution of 0.1 wt % carbopol 940 with the pH adjusted to 4.8 to give a rheology which may be described by the Herschel-Bulkley model,[8]

$$\tau = \tau_y + K\dot{\gamma}^n, \quad (1)$$

where τ is the shear stress, $\dot{\gamma}$ is the shear rate, K is the consistency index, n is the power law exponent, and τ_y is the yield stress. A sample of the fluid was taken before and after each experiment and the parameters in (1) were obtained using a controlled-stress rheometer (Bohlin CVO, Bohlin Instruments). Within ±5%, values of $\tau_y = 1.50$ Pa, $K = 0.16$ Pa s^n, and $n = 0.73$ can be taken for all the samples measured. The fluid density, ρ, was 1000 kgm^{-3}.

Conventional visualization of the cavern boundaries was performed in a glass vessel with $4 \times 90°$ longitudinal baffles of width $0.1T$. A small quantity (1 ml) of nigrosine dye mixed with the vessel contents to a concentration of 1 kg m^{-3} was injected close to the impeller blade before the start of the experiment. The tracer had negligible effect on the fluid rheology. The impeller speed was then set and the cavern was left to stabilize for several minutes. An image was then obtained using a digital camera (Canon Ixus 800, Canon Inc, JP).

PEPI experiments

The cavern boundary was visualized in a steel baffled vessel using PEPI, a 2D variant of positron emission tomography (PET). PET involves the mapping of the concentration of a radioactively labeled species in both space and time. The radioisotope used undergoes β^+ decay, emitting a positron which annihilates with an electron to produce two back to back (within 0.5°) 511 keV γ-rays. These are detected using a PET scanner, from which the concentration field can be reconstructed. In this work, the Birmingham ADAC Forte positron camera[9] was used, which employs two detector heads of size 500×400 mm^2 operating in coincidence: the separation of the heads can be adjusted up to a maximum of 800 mm. Each detector head contains a digital gamma camera comprising a 16 mm thick NaI(Tl) scintillator backed by an array of 55 photomultiplier tubes which are connected to analogue to digital converters and then to a computer. An incident γ ray produces a flash of light which is spread over several photomultiplier tubes; from the registered intensities the centroid is found. Data are recorded when gamma rays are detected in both heads simultaneously. To reconstruct the 3D concentration field using PET it is necessary to measure the number of gamma ray pairs emerging at all angles. Alternatively, using the positron emission particle tracking (PEPT) technique, the camera can be used to track single labeled tracer particles by triangulation of a small number of gamma ray pairs. More information on the employment of both these techniques in process engineering applications is given by Parker et al.[10]

In this work, the steel vessel was placed between the two detectors which were arranged vertically with a separation of 800 mm. The arrangement is as shown in Figure 1 (although depicting the ERT vessel). A small amount of positron-emitting radioactive tracer in the form of $^{18}F^-$ ions was added close to the shaft of the vessel. As in PET, the pairs of back-to-back γ-rays arising from positron/electron annihilations were detected using the Forte camera and used to reconstruct an image, but whereas in PET γ-ray pairs emerging in all directions are used, for PEPI only pairs emerging in one direction (parallel to the camera axis) are exploited. This enables a single side view to be reconstructed, showing the projected area occupied by the tracer. It should be noted that this technique yields no information on the velocity

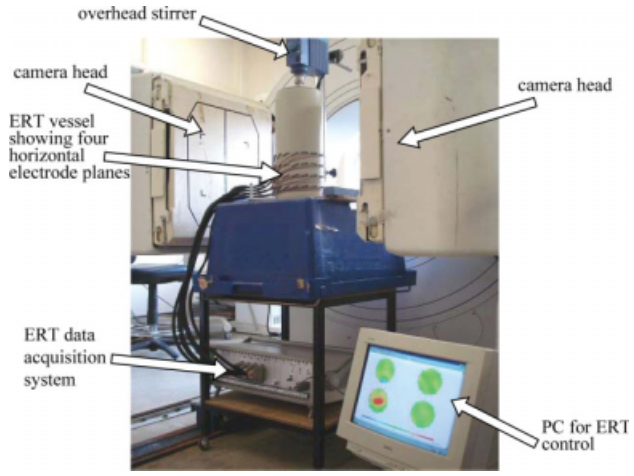

Figure 1. Photograph showing the layout of the ERT vessel and system as installed within the ADAC Forte PET camera during the experiments.

[Color figure can be viewed in the online issue, which is available at www.interscience.wiley.com.]

distribution within the cavern, but simply allows the boundary to be detected. The data were reconstructed into 2 mm square pixels displayed as an eight-bit black and white image (256 gray scale levels), but it should be noted that the intrinsic spatial resolution of the camera is around 6 mm.

ERT experiments

The measurements were performed using a P2000 ERT instrument and vessel [Industrial Tomography Systems (ITS), UK]. The vessel was fitted with a 3D array containing four horizontal planes of 16 electrodes which were connected to the ITS P2000 data acquisition system and a personal computer as shown in Figure 1. The spatial resolution of the system is 5% of the vessel diameter and the data were acquired at two frames per second.

A schematic of the ERT vessel is shown in Figure 2a. In each measurement plane, the 10-mm-square electrodes (manufactured from 316 stainless steel) are placed on an equal pitch around the vessel circumference. The vertical distance between the centers of the electrodes between each plane is 40 mm, with the center of the bottom plane of electrodes being 30 mm from the vessel bottom. The impeller plane is very close to measurement plane three, as shown in Figure 2a. The imaged volume shown by the speckled region in Figure 2a thus occupies a cylinder of diameter equal to T and a height of 120 mm (from the center of the electrodes in plane 1 to the center of the electrodes in plane 4). A plan view of the Cartesian ERT tomogram reconstruction grid is shown in Figure 2b, which splits the vessel into 20 pixels across its diameter (i.e., 5%), giving a resolution of 7.7 mm in the x and y directions. In the vertical z direction there are 19 pixels, hence the resolution is 6.3 mm. The images were reconstructed using the linear back projection algorithm.[4] In the vertical direction, the tomogram was constructed by linear interpolation. The image of the cavern was obtained

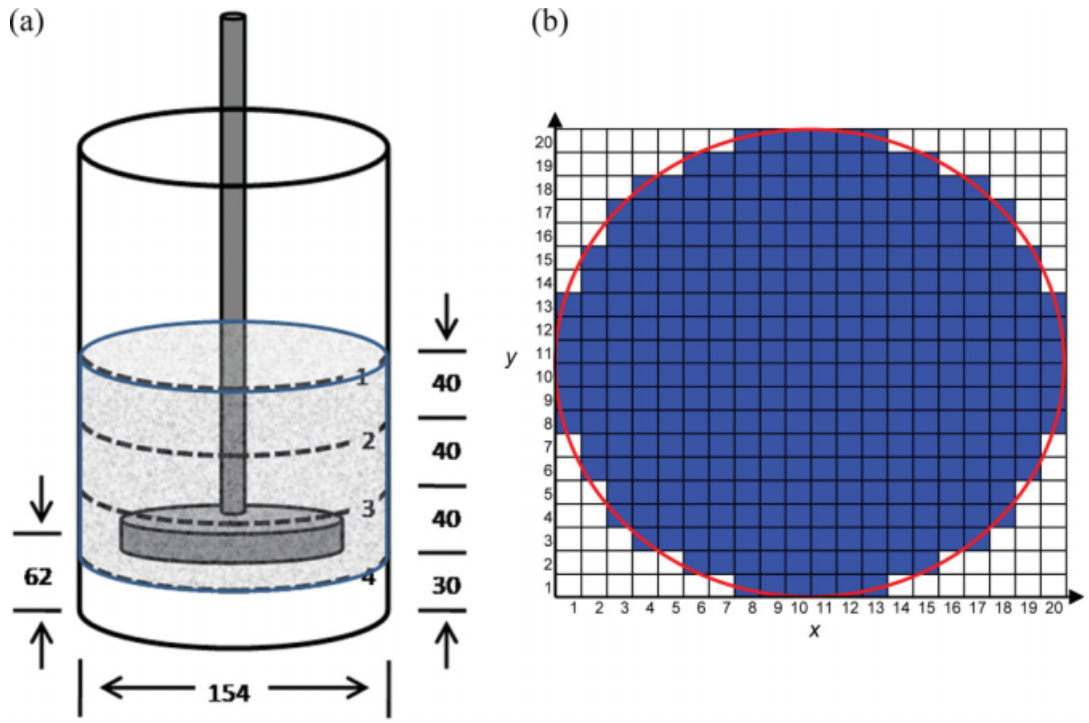

Figure 2. (a) Schematic of ERT vessel showing the four horizontal electrode planes and dimensions, the imaged volume is shown by the speckled region between planes 1 and 4; (b) ERT tomogram reconstruction grid in plan view: all dimensions in mm.

[Color figure can be viewed in the online issue, which is available at www.interscience.wiley.com.]

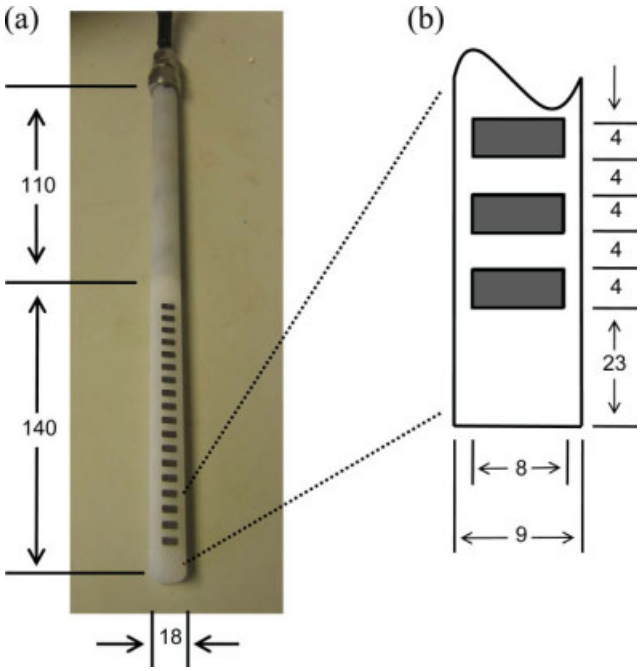

Figure 3. (a) Photograph of ITS linear probe showing critical dimensions; (b) schematic showing dimensions of sensor region: all dimensions in mm.

[Color figure can be viewed in the online issue, which is available at www.interscience.wiley.com.]

by taking longitudinal sections in the x–z plane for each y coordinate, giving 20 sections in total.

An unbaffled vessel was used for the ERT experiments because the specific baffle design employed was found to interfere with the electric field. As the caverns did not extend as far as the baffles, the impact of baffling on the fluid flow is negligible. Two milliliter of 5% NaCl solution was injected at the impeller to increase the local conductivity and "illuminate" the cavern. Although the injection of brine was likely to cause some breakdown of the carbopol structure (which is sensitive to changes in pH or conductivity) causing rheology modification, this is less of an issue in real industrial systems.

An experiment was also performed using a linear electrode array[11] (ITS, UK) instead of the 3D array, a photograph, and schematic of the linear array is given in Figure 3. The array is fabricated from an 18 mm diameter, 250-mm-long polytetrafluoroethylene (PTFE) rod with a 9-mm-flat surface machined onto the side. Eighteen electrodes (316 stainless steel) of size 4×8 mm^2 are located along the rod, spaced 4 mm apart giving an active sensor vertical dimension of 120 mm, and a resolution of 6 mm pixel^{-1} (over 20 pixels). The top and bottom electrodes are earth electrodes with the other 16 being used for acquisition using the same ITS P2000 system. This array was located vertically on the tank wall and faced toward the tank vertical axis, positioned to image the same vertical region as for the 3D sensor array. The robust materials of construction of the probe make it suitable in aggressive chemical and abrasive environments enabling it to be used on process plant.

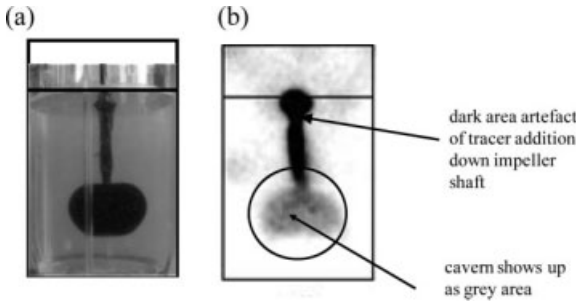

Figure 4. Images of caverns at N = 80 rpm (Re = 20.4) using (a) digital imaging and (b) PEPI technique with key regions indicated.

Results

Cavern boundaries obtained from the digital camera and PEPI are shown in Figure 4 at $N = 80$ rpm. The presence of the cavern is clearly shown by the black region occupying

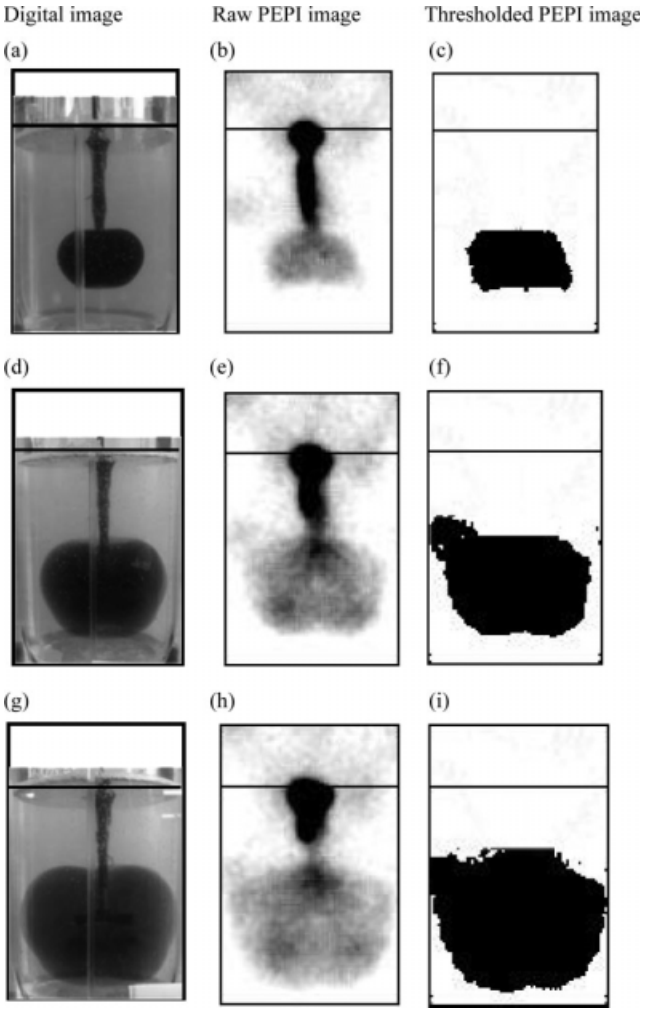

Figure 5. Images of caverns from digital imaging and PEPI technique; images: (a–c) show results at N = 80 rpm (Re = 20.4); (d–f) at N = 162 rpm (Re = 70.3), and (g–i) at N = 207 rpm (Re = 86.6).

Table 1. Comparison of Cavern Dimensions as Measured by Each Technique

Rotational Speed (rpm)	Re	Cavern Projected Area (mm^2)			Max Cavern Width (mm)			Max Cavern Height (mm)		
		Digital Imaging	PEPI	ERT	Digital Imaging	PEPI	ERT	Digital Imaging	PEPI	ERT
80	20.4	3768	4860	3932	80	86	69.3	52	54	69.3
162	70.3	6957	10990	7782	113	128	107.8	90	84	>81.9
207	86.6	11410	14910	–	139	146	–	118	128	–

the impeller in the digital photograph in Figure 4a. Figure 4b shows the corresponding PEPI image, which is dominated by a black area that covers the location of the impeller shaft. This was due to the injection method which caused small quantities of undiluted tracer to leak out of the syringe close to the shaft as the needle was pushed downwards towards the cavern. As the localized mixing near the shaft is very poor, this tracer remained in the vicinity of the shaft for the duration of the experiment. Beneath the shaft region, a grey area corresponding to the spread of the tracer (now diluted with the fluid in the cavern), through the cavern can be observed which is visually of similar size and shape to the cavern shown in Figure 4a.

Further processing of the PEPI images can be performed to obtain the boundary of the extent of the penetration of the radiotracer as obtained from the PEPI reconstruction. The digital image and raw PEPI image at $N = 80$ rpm are again shown in Figures 5a,b. Figure 5c shows the processed image in which the black and grey areas due to the shaft have been removed in the upper part of the image. The remaining image is then thresholded at a gray scale value of 246 to turn all grey regions within the image to black. The penetration of the tracer, assumed to be within the boundaries of the cavern, now appears as the black area. Similar sets of images are shown at increased rotation rates of $N = 162$ rpm (Figures 5d–f) and $N = 207$ rpm (Figures 5g–i) and both digital and PEPI images show the cavern to increase substantially in size, indeed at $N = 162$ and 207 rpm (Figures 5f, i), the cavern is shown to reach the wall of vessel in the mid-left of the PEPI images, although this is not the case in the corresponding digital images (Figures 5d, g). The digital images show that the cavern approximates a toroidal shape, in agreement with the previous study.[8] The corresponding PEPI images (Figures 5f, i) also exhibit a toroidal shape at the bottom of the cavern, although the shape of the top of the caverns is more distorted, possibly due to the dominance of scattered γ-rays from the strong emissions at the shaft.

A quantitative comparison can be made by comparing the magnitude of the cavern projected areas between the digital and PEPI techniques as shown in Table 1. The cavern areas were calculated using freeware image analysis software (Image J). The table shows that the cavern areas obtained via PEPI are 30% larger than from digital images at speeds of $N = 80$ and 207 rpm. At 162 rpm the difference rises to 58%, although clearly comparisons based on area are subject to a squaring of the differences between the measured length scales. The differences can be explained by the presence of the extra area due to the breakthrough to the vessel wall in the mid left of the images shown in Figures 5f, i and distortion close to the top of the caverns due to the shaft. If length-based measurements, i.e., the maximum cavern widths and heights are compared between the two techniques, also shown in Table 1, agreement is much improved and within 10%.

To determine the extent of the cavern from the ERT measurements it is necessary to define the location of the cavern boundary from the measured conductivity profiles. Figure 6a shows the radial profile of the normalized conductivity, (calculated as $\sigma^*(x,y,z) = \sigma(x,y,z)/\sigma_0(x,y,z)$, where σ is the conductivity and σ_0 is the background value measured before injection of the tracer) within the impeller plane at $z = 0.4T$ for 80 and 162 rpm. ERT measurements were not

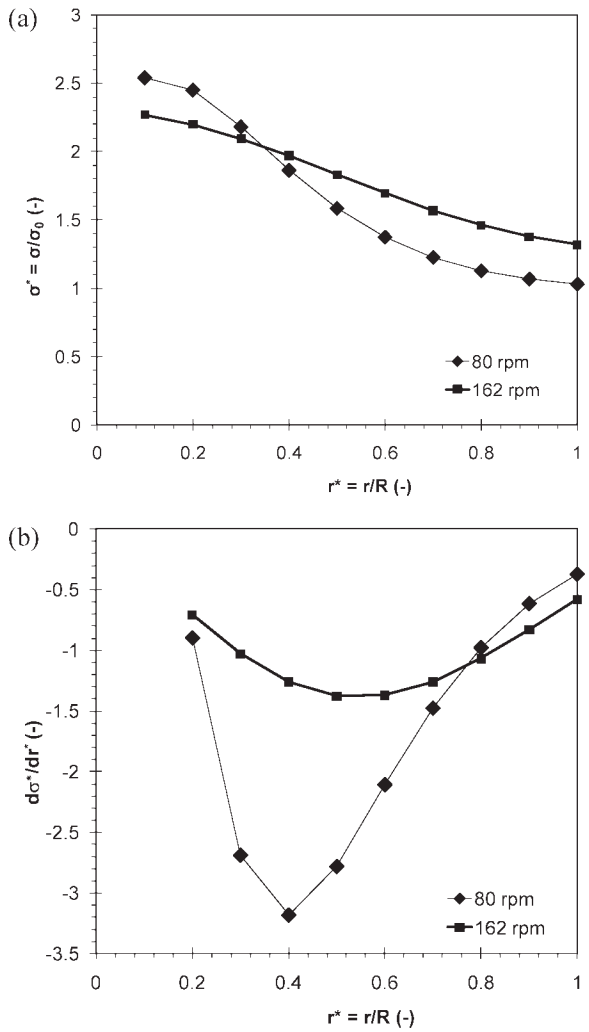

Figure 6. (a) Radial distribution of normalized conductivity, σ^*; (b) rate of change of normalized conductivity with normalized radius, $d\sigma^*/dr^*$, both measured in the impeller plane ($z/T = 0.4$).

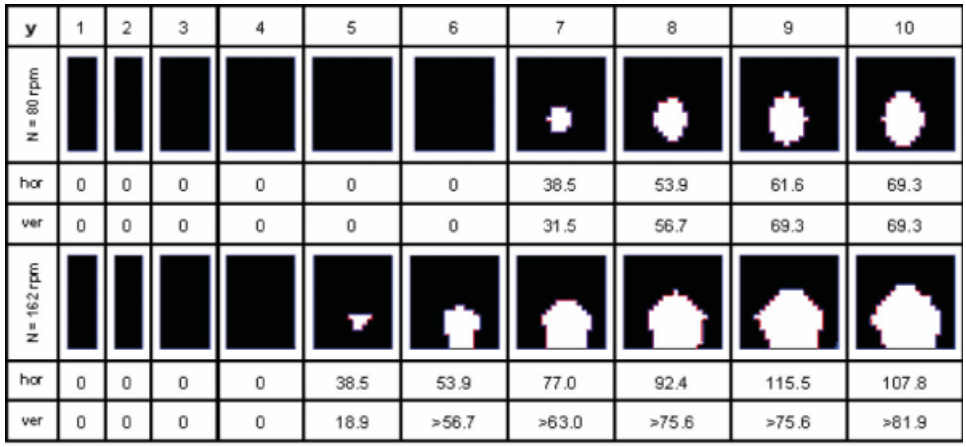

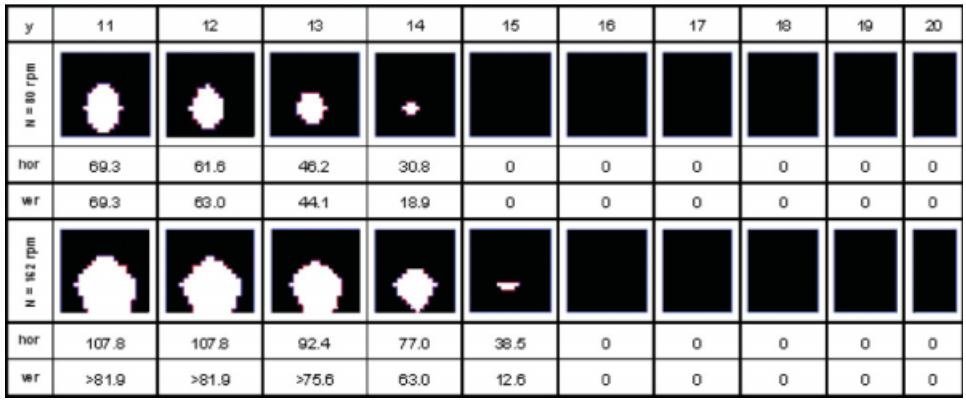

Figure 7. Images of caverns obtained from ERT in each of the 20 slices in the *x* direction at constant *y* position (Figure 2b) for (a) *N* = 80 rpm (Re = 20.4) and (b) *N*= 162 rpm (Re = 70.3).

The caverns appear in white and the "hor" and "ver" rows refer to the maximum horizontal and vertical dimension of the caverns in mm, respectively. [Color figure can be viewed in the online issue, which is available at www.interscience.wiley.com.]

possible at the highest speed used ($N = 207$ rpm) as the tracer became too dilute as it was spread over the bulk of the fluid volume. Values at the vessel axis ($r^* = 0$) have a value of $\sim 2.5\sigma_0$, compared with values of 1.0–1.3 σ_0 at the vessel wall. Although clearly the high conductivity region is due to the presence of the cavern, the profiles are monotonic, with no obvious discontinuity which would directly indicate the presence of the cavern boundary. This is a likely artifact of the reduced sensitivity of the technique near the vessel axis as the density of the electric field lines decrease[4] as well as due to limitations of the linear back projection reconstruction method used.[5]

If the gradient of the normalized conductivity, i.e., $d\sigma^*/dr^*$, is plotted vs. r^*, a minimum is observed at $r^* = 0.4$ and 0.55 for the 80 rpm and 162 rpm data, respectively (Figure 6b), which could perhaps be argued as a reasonable method of locating the cavern boundary. However, the corresponding values of σ^* at these values of r^* are 1.8 and 2.0, respectively, which, even allowing for smoothing of the data due to resolution artifacts, leaves a large amount of conductive material outside the cavern. Therefore, an arbitrary threshold value of $\sigma^* = 1.5$ was chosen. Although choice of different threshold values will clearly change the calculated size of the caverns, the intended application of ERT is for cavern detection on process plant due to the techniques robustness and ease of use. From this viewpoint, ERT is a successful technique although clearly more work is required in terms of image reconstruction and resolution before it can be applied to determine absolute cavern dimensions without reference to another measurement technique.

Using the threshold value of $\sigma^* = 1.5$, images of each of the 20 vertical x–z planes are shown as function of y position at $N = 80$ and $N = 162$ rpm in Figure 7. The area occupied by the cavern appears in white in the black area which corresponds to the fluid within the vessel. No caverns were detected in planes 1–4 or 16–20. Despite its limitations, the advantage of the ERT technique becomes apparent in that 3-D imaging of the cavern is possible. PEPI imaging is 2-D; the images obtained by PEPI are thus a projection. The cavern obtained at 80 rpm is noticeably smaller than that found at 162 rpm, the maximum cavern widths are found as 69 and 108 mm, respectively, in plane 10, which is located across the diameter of the tank. Corresponding cavern heights are 69 and >82 mm, the latter figure is due to the cavern penetrating beneath the region covered by the ERT sensors. Similar results were observed if the reconstruction

is performed to generate 20 vertical y–z planes (as a function of x position) and are not shown.

Comparison of these values with the other two techniques (Table 1) shows that the caverns appear taller and thinner when measured by ERT at the chosen arbitrary threshold, although the measured cavern areas are remarkably close to those obtained by digital imaging. There are two other possible reasons for the difference in shape: first due to some distortion of the electric field causing reduced sensitivity close to the vessel axis and second due to some degree of breakdown of the carbopol structure due to the injection of NaCl tracer. Consequent rheology modification may have increased the extent of the cavern in the vertical direction due to disturbances at the injection point.

The image obtained by the linear array (Figure 8a) shows qualitatively the presence of a cavern (obtained at the same threshold value as for the 3D array), although the degree of penetration of the linear array toward the vessel axis is unknown in these experiments, hence the image has no scale in the radial direction. The small area of high conductivity at the top is due to leakage of brine during injection into the cavern. The numbers on the vertical axis correspond to the number of pixels as detected by the probes. The subplot in Figure 8b shows the average radial conductivity (normalized by the initial value) vs. the number of pixels: the cavern is clearly present at pixel values between 2 and 14. Although this result is more qualitative in nature, it does illustrate the potential of the linear array as a process instrument for cavern detection with ultimate application as a means of in-line process control.

As a means of visual comparison of cavern shape between each technique at the same rotational speed, sketches of the cavern boundaries taken across the diameter of the tank are shown in Figure 9. The sketches highlight the features previously discussed: the caverns as measured by ERT (red) are noticeably taller and narrower, whereas the agreement between the size and shape of the caverns measured by digital imaging (blue) and PEPI (green) are much better. At 162 rpm, the dotted green line indicates where the location of the bottom of the cavern could not be resolved as it dropped below the bottom plane of electrodes.

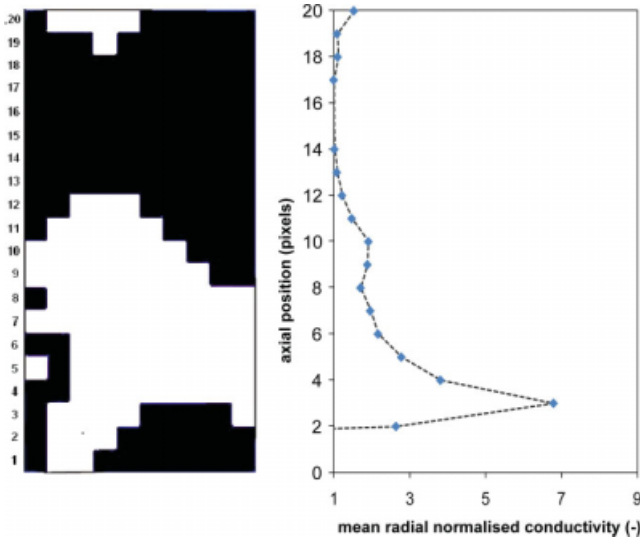

Figure 8. Results from the ITS linear probe at N = 80 rpm (Re = 20.4) using the linear array: (a) reconstructed conductivity image; (b) mean radial normalized conductivity as a function of axial position.

[Color figure can be viewed in the online issue, which is available at www.interscience.wiley.com.]

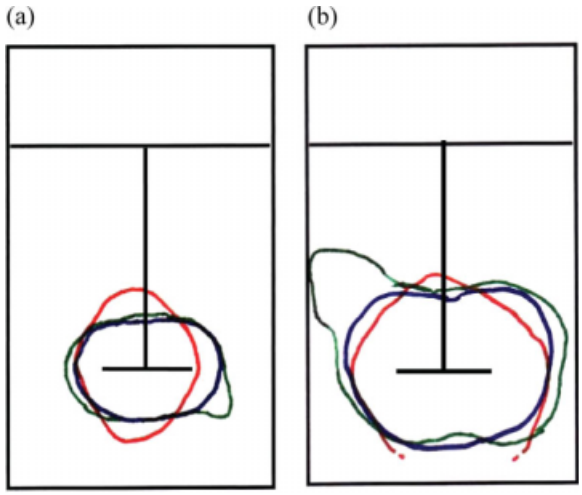

Figure 9. Sketches of the cavern size and shape obtained from each technique: from digital image (blue), PEPI (green) and ERT (red) at (a) N = 80 rpm (Re = 20.4) and (b) N = 162 rpm (Re = 70.3).

Impeller position and liquid free surface shown for reference. [Color figure can be viewed in the online issue, which is available at www.interscience.wiley.com.]

Conclusions

Avoidance of caverns is critical within industrial mixing systems to ensure efficient blending. Two techniques capable of imaging within opaque fluids for cavern detection, PEPI and ERT, have been used to visualize caverns in a transparent aqueous solution of carbopol 940 which exhibits Herschel-Bulkley rheology. Comparison with digital optical images has shown reasonable agreement with PEPI and ERT images taken with a 3D array, despite use of an arbitrary threshold value of conductivity to locate the cavern boundary in the ERT measurements. Although PEPI is mostly a laboratory tool due to the scale and cost of the equipment required and in the use of a radiotracer, the presence of caverns was also found using a robust linear ERT array, which has great potential for cavern detection in process applications due to its chemical resistance and ease of application in process vessels.

Literature Cited

1. Wilkens RJ, Miller JD, Plummer JR, Dietz DC, Myers KJ. New techniques for measuring and modelling cavern dimensions in a Bingham plastic fluid. *Chem Eng Sci*. 2005;60:5269–5275.
2. Elson TP, Cheesman DJ, Nienow AW. X-ray studies of cavern sizes and mixing performance with fluids possessing a yield stress. *Chem Eng Sci*. 1986;41:2555–2562.
3. Saeed S, Ein-Mozaffari F, Upreti SR. Using computational fluid dynamics modelling and ultrasonic doppler velocimetry to study pulp suspension mixing. *Ind Eng Chem Res*. 2007;46:2172–2179.

4. Holden PJ, Wang M, Mann R, Dickin FJ, Edwards RB. Imaging stirred-vessel macromixing using electrical resistance tomography. *AIChE J*. 1998;44:780–790.
5. Bolton GT, Primrose KM. An overview of electrical tomographic measurements in pharmaceutical and related application areas. *AAPS PharmSciTech*. 2005;6:Article 21.
6. Pakzad P, Ein-Mozaffari F, Chan P. Using electrical resistance tomography and computational fluid dynamics modeling to study the formation of cavern in the mixing of pseudoplastic fluids possessing yield stress. *Chem Eng Sci*. 2008:63;2508–2522.
7. Loggia D, Gouze P, Greswell R, Parker DJ. Investigation of the geometrical dispersion regime in a single fracture using positron emission projection imaging. *Transport Porous Media*. 2004;55:1–20.
8. Adams L, Barigou M. CFD analysis of caverns and pseudo-caverns developed during mixing of non-Newtonian fluids. *Chem Eng Res Des*. 2007;85:598–604.
9. Parker DJ, Forster RN, Fowles P, Takhar PS. Positron emission particle tracking using the new Birmingham positron camera. *Nucl Instrum Methods A*. 2002;477:540–545.
10. Parker DJ, Leadbeater TW, Fan X, Hausard MN, Ingram I, Yang Z. Positron imaging techniques for process engineering: recent developments at Birmingham. *Meas Sci Technol*. 2008;19: 094004.
11. Bolton GT. A review of linear electrical tomography probes for monitoring the behaviour of multiphase mixing processes. In: Magelli F, Baldi G, Brucato, A, editors. *Proceedings of the 12th European Conference on Mixing*. Italy: AIDIC, 2006:415–422.

Manuscript received Oct. 16, 2008, and revision received Jan. 22, 2009.